ISA Transactions 152 (2024) 28–37

Contents lists available at ScienceDirect

ISA Transactions

journal homepage: www.elsevier.com/locate/isatrans

Research article

Connectivity preservation control for multiple unmanned aerial vehicles in the presence of bounded actuation

Xianghong Xue [a], Bin Yuan [a], Yingmin Yi [a,*], Youmin Zhang [b], Xiaokui Yue [c], Lingxia Mu [a]

[a] Department of Automation and Information Engineering, Xi'an University of Technology, Xi'an, 710048, China
[b] Department of Mechanical, Industrial and Aerospace Engineering, Concordia University, Montreal, QC H3G 1M8, Canada
[c] National Key Laboratory of Aerospace Flight Dynamics (AFDL), Northwestern Polytechnical University, Xian 710072, China

ARTICLE INFO

Keywords:
Connectivity preservation
Input saturation
Unmanned aerial vehicles
Distributed formation control

ABSTRACT

This paper proposes a novel multi-unmanned aerial vehicle (UAV) connectivity preservation controller, suitable for scenarios with bounded actuation and limited communication range. According to the hierarchical control strategy, controllers are designed separately for the position and attitude subsystems. A distributed position controller is developed, integrating an indirect coupling control mechanism. The innovative mechanism associates each UAV with a virtual proxy, facilitating connections among adjacent UAVs through these proxies. This structuring assists in managing the actuator saturation constraints effectively. The artificial potential function is utilized to preserve network connectivity and fulfill coordination among all virtual proxies. Additionally, an attitude controller designed for finite-time convergence guarantees that the attitude subsystem adheres precisely to the attitude specified by the distributed position controller. Simulation results validate the efficacy of this distributed formation controller with connectivity preservation under bounded actuation conditions. The simulation results confirm the effectiveness of the distributed connectivity preservation controller with bounded actuation.

1. Introduction

Over the past two decades, the deployment of unmanned aerial vehicles (UAVs) has seen significant growth across both military and civilian sectors [1]. The evolution of multiple UAV systems has emerged as an inevitable trend, driven by their potential applications in diverse fields, such as power grid system inspection, forest fire monitoring, search and rescue, crop monitoring, and more [2–7]. Research on the formation control of multiple UAVs has been increasing, highlighted by a notable shift from centralized to distributed control methodologies [8,9]. However, the distributed control of multiple UAVs presents a formidable challenge due to the constraint that each UAV can only access information from its neighboring counterparts.

The communication network should constantly or intermittently be connected to realize distributed control of multiple UAVs. Due to the limited communication range and the relative movements between UAVs, the network's connectivity can be destroyed in practice. Therefore, it is essential to consider network connectivity preservation when designing the distributed control of multiple UAVs. Researchers have explored connectivity preservation controllers within multi-agent systems [10–13]. Connectivity preservation methods can be classified into two types: global and local [14]. In global methods, connectivity is preserved by maximizing algebraic connectivity, a metric used to measure connectivity [15–17]. Local methods preserve the communication network's connectivity by facilitating the exchange of individual position and velocity information between neighboring agents [18,19]. Most of these methods are implemented using artificial potential functions [20,21]. The problem of connectivity preservation for multiple UAVs differs from that of multi-agent systems in two ways. Firstly, while the majority of connectivity preservation control studies in multi-agent systems focus on achieving consensus, the UAV formation issue with connectivity preservation constraints tackles the challenges of formation control. Secondly, while multi-agent systems are generally modeled as linear systems, UAV formation models are nonlinear, adding complexity to the challenge of preserving connectivity in UAV formations. Recently, a study was conducted on a system of multiple quadrotor UAVs to investigate formation control, collision avoidance, and connectivity preservation [22].

When controlling UAVs in practical scenarios, it is crucial to take into account the capabilities of their motors. Specifically, we need to consider the maximum lift force each motor can generate, known as the

* Corresponding author.
E-mail addresses: xhxue@xaut.edu.cn (X. Xue), binyuan@stu.xaut.edu.cn (B. Yuan), yiym@xaut.com (Y. Yi), ymzhang@encs.concordia.ca (Y. Zhang), xkyue@nwpu.edu.cn (X. Yue), lingxiamu@xaut.com (L. Mu).

https://doi.org/10.1016/j.isatra.2024.06.021
Received 14 November 2023; Received in revised form 24 June 2024; Accepted 24 June 2024
Available online 28 June 2024

system's "bounded actuation". It is crucial to ensure that the control algorithm does not generate outputs that exceed this bounded actuation. To prevent overloading the motors, we often use saturation functions that limit the control inputs for one or more UAVs [23]. Backstepping control is commonly used to solve input saturation problems for a single UAV [24–26]. Eliker et al. developed a UAV input saturation controller using a sliding mode controller and a backstepping method with a saturation compensator [27]. Literature [28] implemented an adaptive finite-time control law and constructed an improved hyperbolic function-assisted dynamical system to tackle the issue of input saturation, allowing for the finite-time convergence of tracking errors. Despite these advances, studies on connectivity preserving control under conditions of input saturation remain rare in the existing literature.

The current challenge is to develop distributed controllers for UAVs while ensuring both connectivity preservation and bounded actuation. Inspired by the literature [29–31], this paper presents a distributed controller with connectivity preservation under bounded actuation and limited communication distances. In line with the hierarchical control strategy, separate controllers are designed for the position and attitude subsystems. A distributed position controller is developed, integrating an indirect coupling control mechanism. The innovative mechanism associates each UAV with a virtual proxy, facilitating connections among adjacent UAVs through these proxies. These UAV–proxy couplings are instrumental in managing the actuator saturation constraints. The potential function comes into play to ensure network connectivity and coordination among all the virtual proxies. To guarantee the accurate following of the desired attitude set by the distributed position controller, we develop an attitude controller with finite-time convergence. The simulation results affirm the effectiveness of our approach, demonstrating the successful operation of the distributed connectivity preservation controller with bounded actuation.

The key contributions are summarized as follows:

(1) In this study, we develop a distributed formation control strategy for a group of UAVs, which is fundamentally based on the boundary barrier function. This method not only preserves the connectivity of the topological network but also prevents collisions between UAVs, all while taking into account the communication distance constraint.
(2) Many studies have only considered either the multiple UAVs connectivity preservation problem or the multiple UAVs input saturation control problem individually, while very few studies have considered both at the same time. This study presents a distributed controller indirect coupling mechanism. The primary goal of this approach is to tackle the challenges associated with connectivity preservation and input saturation in multi-UAV systems.
(3) We present a distributed formation control framework that combines inner- and outer-loop control with virtual UAVs. This framework is well suited to realize the distributed controllers in this paper.

The structure of this paper is as follows: Section 2 outlines the relative dynamics of UAV, the communication model, and the problem statement. Section 3.1 introduces the connectivity preservation controllers for the positioning subsystem. In Section 3.2, we present a finite-time attitude-tracking controller. Simulation results are presented in 4. The study concludes with some final remarks in Section 5.

2. Problem statement

2.1. Dynamical model

This paper explores the issue of formation control for a group of N quadrotor UAVs. Let us consider the inertial frame $\mathcal{F}_I = \{O_I x_I y_I z_I\}$, with its origin O_I anchored at a certain point on the earth. The states of a UAV are depicted as

$$\left(x_i, y_i, z_i, \phi_i, \theta_i, \psi_i\right)^T \in \mathbb{R}^6, \quad i \in \Gamma,$$

where $\boldsymbol{\Phi} = [\phi_i, \theta_i, \psi_i]^T$ denotes UAV i's attitude relative to $\mathcal{F}_I$ and $\boldsymbol{p}_i = [x_i, y_i, z_i]^T$ refers UAV i' position concerning $\mathcal{F}_I$.

(1) Position dynamics

The dynamics of UAV i is modeled as [32]

$$m_i \ddot{\boldsymbol{p}}_i = -m_i g \boldsymbol{e}_3 + T_i \boldsymbol{R}_i \boldsymbol{e}_3, \tag{1}$$

where m_i denotes UAV i' total mass, $\boldsymbol{e}_3 = [0, 0, 1]^T$, $g = 9.81\ \mathrm{m/s^2}$, T_i represents the total lift, the rotation matrix $\boldsymbol{R}_i$ is given as follows

$$\boldsymbol{R}_i = \begin{bmatrix} \theta_i^c \psi_i^c & \theta_i^s \psi_i^c \phi_i^s - \psi_i^s \phi_i^c & \theta_i^s \psi_i^c \phi_i^c + \psi_i^s \phi_i^s \\ \theta_i^c \psi_i^s & \theta_i^s \psi_i^s \phi_i^s + \psi_i^c \phi_i^c & \theta_i^s \psi_i^s \phi_i^c - \psi_i^c \phi_i^s \\ -\theta_i^s & \theta_i^c \phi_i^s & \theta_i^c \phi_i^c \end{bmatrix}, \tag{2}$$

where $\theta_i^c = \cos\theta_i, \theta_i^s = \sin\theta_i$, $\psi_i^c = \cos\psi_i, \psi_i^s = \sin\psi_i$, $\phi_i^c = \cos\phi_i, \phi_i^s = \sin\phi_i$.

Eq. (1) shows that the position dynamics equation is attitude-dependent, making it challenging to design a controller that simultaneously considers both position and attitude. Consequently, the attitude can be replaced by a virtual control input [33]. Denote

$$T_i \boldsymbol{R}_i \boldsymbol{e}_3 := \boldsymbol{u}_i(t), \tag{3}$$

and Eq. (1) can be rewritten as

$$m_i \ddot{\boldsymbol{p}}_i = -m_i g \boldsymbol{e}_3 + \boldsymbol{u}_i(t). \tag{4}$$

Remark 1. The separation of attitude dynamics and position dynamics is facilitated by using Eq. (3). This results in the quadrotor UAV exhibiting inner-loop attitude dynamics and outer-loop position dynamics. Through the use of this decoupling approach, the inner and outer-loop dynamics can be independently managed. This separation allows for the direct design of the controller based on dynamics Eq. (4), which supports the preservation of network connectivity and the realization of the desired configuration. The desired lift and attitudes can then be determined based on Eq. (3), with the solution presented in Eq. (25). Subsequently, an attitude-tracking controller is developed to accurately follow the specified attitude. Fig. 1 depicts the control block diagram. The decoupling methodology is detailed in the referenced literature [33,34] and validated through experiments.

(2) Attitude dynamics

Similarly, the attitude angular $\boldsymbol{\Phi}_i = [\phi_i, \theta_i, \psi_i]^T$ and attitude angular velocity $\boldsymbol{\omega}_i = [\dot{\phi}_i, \dot{\theta}_i, \dot{\psi}_i]^T$ are described in $\mathcal{F}_I$. The ith UAV's attitude dynamics can be modeled as follows:

$$\begin{aligned} J_{i,\phi} \ddot{\phi}_i &= -K_{i,\phi} l_i \dot{\phi}_i + l_i \tau_{i,\phi}, \\ J_{i,\theta} \ddot{\theta}_i &= -K_{i,\theta} l_i \dot{\theta}_i + l_i \tau_{i,\theta}, \\ J_{i,\psi} \ddot{\psi}_i &= -K_{i,\psi} \dot{\psi}_i + c_i \tau_{i,\psi}. \end{aligned} \tag{5}$$

where $J_{i,\phi}, J_{i,\theta}, J_{i,\psi} \in \mathbb{R}^+$ represents UAV i's moments of inertia, $K_{i,\phi}, K_{i,\theta}, K_{i,\psi} \in \mathbb{R}^+$ denotes the aerodynamic damping coefficients, $l_i \in \mathbb{R}^3$ indicates the distance between the rotor shaft center and the epicenter of the UAV, $c_i \in \mathbb{R}^+$ denotes a constant force-to-moment factor, $\tau_{i,\phi}$, $\tau_{i,\theta}$ and $\tau_{i,\psi}$ denote three control torques generated by the rotors.

2.2. Communications model

The communication links among all UAVs can be represented as a proximity graph based on distance. This proximity graph, denoted as $\mathcal{G}(\mathcal{V}, \mathcal{E})$, has a vertex set $\mathcal{V} = \{1, 2, \ldots, N\}$ and an edge set $\mathcal{E} \subset \mathcal{V} \times \mathcal{V}$. A graph $\mathcal{G}$ is called connected if there is a path between any two vertices in $\mathcal{V}$ [35]. In this context, the vertex set represents the UAVs, and the edge set symbolizes the communication links among them. The

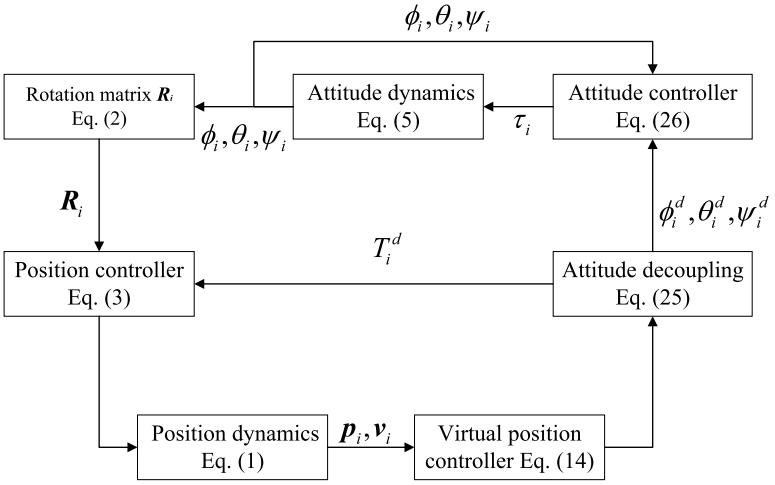

Fig. 1. The control block diagram of the decoupling framework.

adjacency matrix $\boldsymbol{A}(\mathcal{G})$ representing the connections between all UAVs is provided as follows:

$$a_{ij}(t) = \begin{cases} 1, & \text{if } \|\boldsymbol{p}_{ij}(t)\| \le \bar{\Delta}, i, j \in \mathcal{V} \\ 0, & \text{otherwise} \end{cases} \tag{6}$$

where $\boldsymbol{p}_{ij}(t) = \boldsymbol{p}_i(t) - \boldsymbol{p}_j(t)$, $\bar{\Delta} = \Delta - \nu$ where $\nu > 0$ is a tiny constant, Δ denotes the communication distance of UAV i.

By using $\boldsymbol{A}(\mathcal{G})$, the Laplacian matrix $\boldsymbol{L}(\mathcal{G}) = [l_{ij}] \in \mathbb{R}^{N\times N}$ can be written as

$$l_{ij} = \begin{cases} \sum_{j=1}^{N} a_{ij}, & \text{if } i = j \\ -a_{ij}, & \text{otherwise.} \end{cases}$$

The Laplacian matrix is crucial for designing distributed formation controllers for multi-agent systems. We will utilize it to analyze the convergence of the proposed controller.

Remark 2. Most traditional distributed formation control methods assume the communication network is always connected. However, this paper considers the constraint of communication distance, where the communication network is defined based on the relative distance and communication range between UAVs. As a result, the distance constraint must be addressed when designing a distributed formation controller.

Remark 3. In this paper, we select a distance $\bar{\Delta}$ slightly less than the actual communication distance Δ as the condition for establishing the topology link. The purpose is to ensure that the control inputs, subject to the actuator's saturation constraints, preserve the network's connectivity.

Remark 4. In this paper, the number of edges is determined by calculating the edges of the initial network. In the most conservative scenario, where the topological network forms a complete graph, the maximum value of M equals $\frac{N(N-1)}{2}$.

2.3. Control objectives

This paper develops a distributed control law that allows multiple UAVs to preserve the network's connectivity and achieve the desired formation configuration, all within the constraints of bounded actuation. The above two subsections introduce the dynamics and the communication model of the network. To proceed, we must establish the following reasonable assumptions.

Assumption 1. The graph $\mathcal{G}(0)$ determined by the initial conditions is connected.

Assumption 2. All UAVs have an initial velocity of zero, i.e., $\dot{\boldsymbol{p}}_i(0) = 0$.

Assumption 3. The desired configuration, $\boldsymbol{p}_d$, meets the following conditions

$$\|\boldsymbol{p}_i^d - \boldsymbol{p}_j^d\| < \bar{\Delta}, \forall i \in \{1, \dots, N\}, j \in \mathcal{N}_i.$$

Assumption 4. The boundary of the saturation function can completely balance the gravity of each UAV $m_i g$ in Eq. (4), i.e., $\bar{u}_{i,z} \ge |m_i g|$, where $\bar{u}_{i,z}$ denotes the maximum allowed virtual control input for UAV i in the upward direction.

Remark 5. From the results in [29,31] one knows Assumptions 1 and 4 is reasonable. Assumption 3, which guarantees the desired formation is achievable, is also supported by [30] Preserving the connectivity of a second-order system while using bounded control inputs, as described in equation ((4)), is generally considered infeasible. An example demonstrating this challenge can be found in [31]. Therefore, Assumption 2 is reasonable.

Remark 6. This paper sets the input saturation's upper limit based on the maximum virtual control force, which is derived from the upper limit of the lift force. The lift force can be expressed as follows:

$$T_i = m_i \sqrt{u_{i,x}^2 + u_{i,y}^2 + u_{i,z}^2}.$$

During horizontal formation, $u_{i,z} + g = 0$, it can be obtained that

$$(\frac{T_i}{m_i})^2 = u_{ix}^2 + u_{iy}^2 + g^2. \tag{7}$$

Assuming an equal maximum virtual control force in the horizontal direction, the upper limit of the virtual control input correlates with the upper limit of the lift as follows

$$\bar{u}_{i,x} = \bar{u}_{i,y} = \frac{\sqrt{\bar{T}_i^2 - m_i^2 g^2}}{\sqrt{2} m_i}. \tag{8}$$

Hence, the limits of the virtual control force can be determined based on the limits of the lift force. This allows the use of a virtual control force with an upper limit instead of that of a real lift force.

The primary objectives of this study are as follows: (1) achieving the desired formation configuration; (2) all UAV's velocities converge to zero; (3) the graph's connectivity can be preserved; (4) the control inputs meet the input saturation constraints. We have also added a remark for the problem formulation. Based on the above introduction, the problem is modeled as follows.

Problem 1. Given the system (4) and the communication graph described in (6) with Assumptions 1–4, design a distributed controller $\boldsymbol{u}_i$ to reach the following objectives:

(1) the distances between UAVs converge to that of the desired configuration, i.e., $\|\boldsymbol{p}_{ij}(t)\| \to \|\boldsymbol{p}_i^d - \boldsymbol{p}_j^d\|, (i,j) \in \mathcal{E}$.
(2) preserving the graph's connectivity, i.e., $\left\|\boldsymbol{p}_{ij}(0)\right\| < \bar{\Delta}$, then $\left\|\boldsymbol{p}_{ij}(t)\right\| < \Delta, \forall t > 0, (i,j) \in \mathcal{E}$,
(3) the velocities of UAVs reduce to zero, i.e., $\dot{\boldsymbol{p}}_i(t)$ as $t \to \infty$,
(4) the control inputs meet the input saturation constraints, i.e., $\|\boldsymbol{u}_i\| \le \bar{u}_i$.

Remark 7. In the problem description, we have only taken into account positional dynamics. The solution to Problem 1 ensures that the UAVs can realize the desired configuration when the actual control inputs are equal to the virtual control inputs. The desired attitude is calculated using the virtual control inputs. Finally, a finite-time attitude controller is developed.

2.4. Related lemmas

For the controller design and stability analysis, the following lemmas are required.

Lemma 1 ([35]). *The Laplacian matrix $\boldsymbol{L}(\mathcal{G})$ is positive semi-definite, provided that graph $\mathcal{G}$ is connected.*

Lemma 2 ([36]). *Consider the following system*

$$\dot{\xi} = f(\xi) + \hat{f}(\xi), \quad f(\mathbf{0}) = 0, \ \xi \in \mathbb{R}^n,$$

where $f(\xi)$ is a continuous homogeneous vector field of degree $k < 0$ with respect to $(r_1, \ldots, r_n)$, and $\hat{f}$ satisfies $\hat{f}(\mathbf{0}) = 0$. Assume $\xi = 0$ is an asymptotically stable equilibrium of the system $\dot{\xi} = f(\xi)$. Then $\xi = \mathbf{0}$ is a locally finite-time stable equilibrium of the system if

$$\lim_{\epsilon \to 0} \frac{\hat{f}_i\left(\epsilon^{r_1}\xi_1, \ldots, \epsilon^{r_n}\xi_n\right)}{\epsilon^{k+r_i}} = 0, \quad i = 1, \ldots, n, \forall \xi \neq \mathbf{0}.$$

3. Controller design

The design of the connectivity preservation controller includes two components: a position controller with bounded actuation and an attitude-tracking controller. Fig. 2 shows the working process of the proposed connectivity preservation controllers.

3.1. Design of coordination controller for positional control with bounded actuation

The formation controller is developed with an indirect coupling framework: (1) Each UAV is equipped with a virtual proxy; (2) The proxies establish connections reflecting the communication links between their respective UAVs.

Let $\hat{\boldsymbol{p}}_i$ denote the position of virtual proxy i, the dynamics is designed as follows

$$\begin{aligned} &\hat{\boldsymbol{p}}_i(0) = \boldsymbol{p}_i(0), \ \dot{\hat{\boldsymbol{p}}}_i(0) = 0, \\ &\ddot{\hat{\boldsymbol{p}}}_i = \mathrm{Sat}_i\left(\alpha_i \tilde{\boldsymbol{p}}_i\right) - \sum_{j=1}^{N} a_{ij} \nabla_i \Psi\left(\|\hat{\boldsymbol{p}}_{ij}\|\right) - \sum_{j=1}^{N} a_{ij}\left(\dot{\hat{\boldsymbol{p}}}_i - \dot{\hat{\boldsymbol{p}}}_j\right) - \beta_i \dot{\tilde{\boldsymbol{p}}}_i, \end{aligned} \tag{9}$$

where α_i, β_i and η_i denote positive constants, $\mathrm{Sat}_i(\boldsymbol{x}) \in \mathbb{R}^3$ is a function that applies component-wise saturation to $\boldsymbol{x}$ with upper bound $\bar{u}_{i,k}, k = 1,2,3$. Then, the UAV–proxy error can be written as:

$$\tilde{\boldsymbol{p}}_i = \boldsymbol{p}_i - \hat{\boldsymbol{p}}_i \tag{10}$$

The distance-based bounded potential function $\Psi\left(\left\|\hat{\boldsymbol{p}}_{ij}\right\|\right)$ is presented as:

$$\Psi\left(\left\|\hat{\boldsymbol{p}}_{ij}\right\|\right) = \begin{cases} P\Psi^f\left(\left\|\hat{\boldsymbol{p}}_{ij}\right\|\right), & \text{if } \|\hat{\boldsymbol{p}}_{ij}\| \in [0, d_{ij}] \\ P\Psi^c\left(\left\|\hat{\boldsymbol{p}}_{ij}\right\|\right), & \text{if } \|\hat{\boldsymbol{p}}_{ij}\| \in [d_{ij}, \hat{\Delta}] \end{cases} \tag{11}$$

where the formation potential function $\Psi^f\left(\left\|\hat{\boldsymbol{p}}_{ij}\right\|\right)$ and the connectivity preservation potential function $\Psi^c\left(\left\|\hat{\boldsymbol{p}}_{ij}\right\|\right)$ are designed as

$$\Psi^f\left(\left\|\hat{\boldsymbol{p}}_{ij}\right\|\right) = \frac{\left(\left\|\hat{\boldsymbol{p}}_{ij}\right\| - d_{ij}\right)^2\left(\hat{\Delta} - \left\|\hat{\boldsymbol{p}}_{ij}\right\|\right)}{\left\|\hat{\boldsymbol{p}}_{ij}\right\| + \frac{d_{ij}^2\left(\hat{\Delta} - \left\|\hat{\boldsymbol{p}}_{ij}\right\|\right)}{Q}},$$

$$\Psi^c\left(\left\|\hat{\boldsymbol{p}}_{ij}\right\|\right) = \frac{\left\|\hat{\boldsymbol{p}}_{ij}\right\|\left(\left\|\hat{\boldsymbol{p}}_{ij}\right\| - d_{ij}\right)^2}{\left(\hat{\Delta} - \left\|\hat{\boldsymbol{p}}_{ij}\right\|\right) + \frac{\left\|\hat{\boldsymbol{p}}_{ij}\right\|(\hat{\Delta} - d_{ij})^2}{Q}},$$

where $\hat{\Delta} = \Delta - \epsilon$, $\epsilon > 0$ is a small constant. d_{ij} is the desired distance. P, Q are the potential function coefficients.

Remark 8. It can be straightforwardly established that the potential function Φ exhibits a monotonic increase when $\|\hat{\boldsymbol{p}}_{ij}\| \in (d_{ij}, \hat{\Delta})$, and a monotonic decrease when $\|\hat{\boldsymbol{p}}_{ij}\| \in (0, d_{ij})$. Consequently, the potential function achieves its minimum value when $\|\hat{\boldsymbol{p}}_{ij}\| = d_{ij}$.

Remark 9. To ensure that $\left\|\boldsymbol{p}_{ij}\right\|$ falls within the range $(0, \Delta]$ for every edge (i,j) in the edge set $\mathcal{E}$, it suffices that the following conditions are met:

$$\left\|\hat{\boldsymbol{p}}_{ij}\right\| \le \hat{\Delta}, \ \|\tilde{\boldsymbol{p}}_i\| \le \epsilon/2, \ \left\|\tilde{\boldsymbol{p}}_j\right\| \le \epsilon/2.$$

where $\left\|\boldsymbol{p}_{ij}\right\| \le \|\tilde{\boldsymbol{p}}_i\| + \left\|\hat{\boldsymbol{p}}_{ij}\right\| + \left\|\tilde{\boldsymbol{p}}_j\right\|$ is employed.

Lemma 3 ([37]). *Let $\lambda_i\left(\tilde{\boldsymbol{p}}_i\right) = \int_0^{\tilde{\boldsymbol{p}}_i} \mathrm{Sat}_i\left(\alpha_i \sigma\right)^T d\sigma$ represents the relationship between UAV i and its virtual proxy, the following properties are observed:*

(1) *The function $\lambda_i\left(\tilde{\boldsymbol{p}}_i\right)$ is a convex.*
(2) *The function $\lambda_i\left(\tilde{\boldsymbol{p}}_i\right)$ attains its maximum value when $\left\|\tilde{\boldsymbol{p}}_i\right\| = (\epsilon/2)$, and its minimum value when $\left\|\tilde{\boldsymbol{p}}_i\right\| = 0$ in the domain of $B(\mathbf{0}, (\epsilon/2)) = \{\tilde{\boldsymbol{p}}_i \mid \|\tilde{\boldsymbol{p}}_i\| \le (\epsilon/2)\}$, .*
(3) *If $\lambda_i\left(\tilde{\boldsymbol{p}}_i\right) \le \lambda_i^{\min}$, where*

$$\lambda_i^{\min} = \min_{\tilde{\boldsymbol{p}}_i} \ \lambda_i\left(\tilde{\boldsymbol{p}}_i\right), \ s.t. \ \left\|\tilde{\boldsymbol{p}}_i\right\| = \frac{\epsilon}{2}, \tag{12}$$

then $\tilde{\boldsymbol{p}}_i \in B(\mathbf{0}, (\epsilon/2))$.

With the dynamics of the proxies, the distributed formation controller is developed as follows

$$\boldsymbol{u}_i = -\mathrm{Sat}_i(\alpha_i \tilde{\boldsymbol{p}}_i) + m_i g \boldsymbol{e}_3. \tag{13}$$

Theorem 1. *Consider the system defined in Eq. (4), giving the controller (13) with Assumptions 1–4. Let $M = |\mathcal{E}(0)|$, and select Q and P satisfy*

$$Q \ge M\Psi(\bar{\Delta}), \tag{14}$$

$$P = \frac{\min_{i=1,\ldots,N}\{\lambda_i^{\min}\}}{Q}. \tag{15}$$

Then, Problem 1 is solved.

Proof. Design the following Lyapunov function

$$V = V_1 + V_2, \tag{16}$$

where

$$V_1 = \frac{1}{2}\sum_{i=1}^{N}\left(\dot{\boldsymbol{p}}_i^T m_i \dot{\boldsymbol{p}}_i + \dot{\tilde{\boldsymbol{p}}}_i^T \dot{\tilde{\boldsymbol{p}}}_i\right), \tag{17}$$

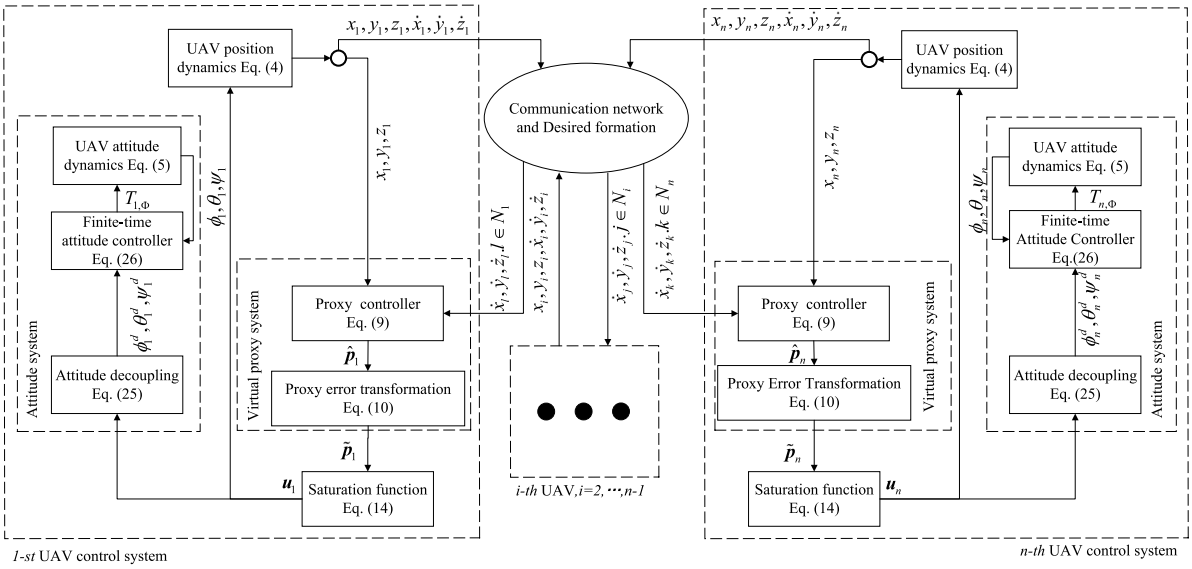

Fig. 2. Working process of the proposed controllers.

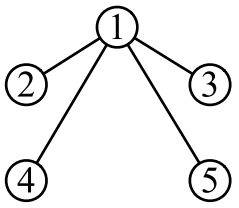

Fig. 3. The communication graph $\mathcal{G}$ of the five UAVs.

$$V_2 = \frac{1}{2}\sum_{i=1}^{N}\sum_{j=1}^{N} a_{ij}\Psi\left(\left\|\hat{\boldsymbol{p}}_{ij}\right\|\right) + \sum_{i=1}^{N}\lambda_i\left(\tilde{\boldsymbol{p}}_i\right). \tag{18}$$

Step 1: Analysis of stability

By differentiating Eq. (17) and using Eqs. (4), (9) and (13), one can obtain

$$\begin{aligned}\dot{V}_1(t) =& \sum_{i=1}^{N}\dot{\boldsymbol{p}}_i^T\left[-m_i g\boldsymbol{e}_3 - \mathrm{Sat}_i(\alpha_i\tilde{\boldsymbol{p}}_i) + m_i g\boldsymbol{e}_3\right]\\ &+ \sum_{i=1}^{N}\dot{\hat{\boldsymbol{p}}}_i^T\left[\mathrm{Sat}_i\left(\alpha_i\tilde{\boldsymbol{p}}_i\right) - \sum_{j=1}^{N} a_{ij}\nabla_i\Psi\left(\|\hat{\boldsymbol{p}}_{ij}\|\right)\right.\\ &\left. - \sum_{j=1}^{N} a_{ij}\left(\dot{\hat{\boldsymbol{p}}}_i - \dot{\hat{\boldsymbol{p}}}_j\right) - \beta_i\dot{\hat{\boldsymbol{p}}}_i\right]\\ =& -\sum_{i=1}^{N}\dot{\hat{\boldsymbol{p}}}_i^T\,\mathrm{Sat}_i(\alpha_i\tilde{\boldsymbol{p}}_i) - \sum_{i=1}^{N}\sum_{j=1}^{N} a_{ij}\dot{\hat{\boldsymbol{p}}}_i^T\nabla_i\Psi\left(\|\hat{\boldsymbol{p}}_{ij}\|\right)\\ &- \sum_{i=1}^{N}\sum_{j=1}^{N} a_{ij}\dot{\hat{\boldsymbol{p}}}_i^T\left(\dot{\hat{\boldsymbol{p}}}_i - \dot{\hat{\boldsymbol{p}}}_j\right)\\ &- \beta_i\sum_{i=1}^{N}\dot{\hat{\boldsymbol{p}}}_i^T\dot{\hat{\boldsymbol{p}}}_i.\end{aligned} \tag{19}$$

The representation of the derivative of V_2 in Eq. (18) can be expressed as

$$\begin{aligned}\dot{V}_2(t) =& \frac{1}{2}\sum_{i=1}^{N}\sum_{j=1}^{N} a_{ij}\left[\nabla_i\Psi\left(\left\|\hat{\boldsymbol{p}}_{ij}\right\|\right)\dot{\hat{\boldsymbol{p}}}_i + \nabla_j\Psi\left(\left\|\hat{\boldsymbol{p}}_{ij}\right\|\right)\dot{\hat{\boldsymbol{p}}}_j\right] + \sum_{i=1}^{N}\dot{\tilde{\boldsymbol{p}}}_i^T\,\mathrm{Sat}_i(\alpha_i\tilde{\boldsymbol{p}}_i)\\ =& \sum_{i=1}^{N}\sum_{j=1}^{N} a_{ij}\dot{\hat{\boldsymbol{p}}}_i^T\nabla_i\Psi\left(\left\|\hat{\boldsymbol{p}}_{ij}\right\|\right) + \sum_{i=1}^{N}\dot{\tilde{\boldsymbol{p}}}_i^T\,\mathrm{Sat}_i(\alpha_i\tilde{\boldsymbol{p}}_i).\end{aligned} \tag{20}$$

By using Eqs. (19) and (20), one has

$$\begin{aligned}\dot{V}(t) =& -\sum_{i=1}^{N}\dot{\hat{\boldsymbol{p}}}_i^T\,\mathrm{Sat}_i(\alpha_i\tilde{\boldsymbol{p}}_i) - \sum_{i=1}^{N}\dot{\hat{\boldsymbol{p}}}_i^T\sum_{j=1}^{N} a_{ij}\nabla_i\Psi\left(\|\hat{\boldsymbol{p}}_{ij}\|\right)\\ &- \sum_{i=1}^{N}\sum_{j=1}^{N} a_{ij}\dot{\hat{\boldsymbol{p}}}_i^T\left(\dot{\hat{\boldsymbol{p}}}_i - \dot{\hat{\boldsymbol{p}}}_j\right)\\ &- \beta_i\sum_{i=1}^{N}\dot{\hat{\boldsymbol{p}}}_i^T\dot{\hat{\boldsymbol{p}}}_i + \sum_{i=1}^{N}\sum_{j=1}^{N} a_{ij}\nabla_i\Psi\left(\left\|\hat{\boldsymbol{p}}_{ij}\right\|\right)\dot{\hat{\boldsymbol{p}}}_i + \sum_{i=1}^{N}\dot{\tilde{\boldsymbol{p}}}_i^T\,\mathrm{Sat}_i(\alpha_i\tilde{\boldsymbol{p}}_i)\\ =& -\beta_i\sum_{i=1}^{N}\dot{\hat{\boldsymbol{p}}}_i^T\dot{\hat{\boldsymbol{p}}}_i.\end{aligned} \tag{21}$$

According to (21), one has $\dot{V}(t) \le 0$ and $V(t) \le V(0)$. It is obtained from Eq. (21) that $\dot{\boldsymbol{p}}_i, \Phi(\hat{\boldsymbol{p}}_i), \lambda(\tilde{\boldsymbol{p}}_i) \in \mathcal{L}_\infty$ and $\dot{\hat{\boldsymbol{p}}}_i \in \mathcal{L}_2 \cap \mathcal{L}_\infty$. Consequently, $\dot{\hat{\boldsymbol{p}}}_i$ converges to $\boldsymbol{0}$ as t tends to infinity. Since $\Psi(\hat{\boldsymbol{p}}_i)$ is continuously differentiable and bounded, we have $\nabla_i\Psi(\hat{\boldsymbol{p}}_i) \in \mathcal{L}_\infty$. Differentiating Eq. (9) suggests that $\ddot{\tilde{\boldsymbol{p}}}_i \in \mathcal{L}_\infty$ and $\ddot{\hat{\boldsymbol{p}}}_i$ converges to $\boldsymbol{0}$ as t tends to infinity. The secondary derivative of Eq. (9) further indicates $\dddot{\tilde{\boldsymbol{p}}}_i$ converges to $\boldsymbol{0}$ as t tends to infinity. Thus, $\ddot{\boldsymbol{p}}_i$ and $\nabla_i\Psi(\|\hat{\boldsymbol{p}}_i\|)$ converges to $\boldsymbol{0}$ as t tends to infinity. The definition of the potential function ensures that $\|\hat{\boldsymbol{p}}_i\| \to d_{ij}$. Noting that both $\ddot{\tilde{\boldsymbol{p}}}_i$ and $\ddot{\hat{\boldsymbol{p}}}_i$ converge to $\boldsymbol{0}$, Eq. (9) concludes that $\ddot{\tilde{\boldsymbol{p}}}_i$ converges to $\boldsymbol{0}$ as t tends to infinity. Overall, $\|\boldsymbol{p}_i\|$ converges to d_{ij} for all $(i,j) \in \mathcal{E}$ as t tends to infinity, thus achieving the desired configuration.

Step 2: Analysis of connectivity preservation

Given the initial conditions specified in Eq. (9) and Assumption 2, we determine $V_1(0) = 0$ and $\psi_i\left(\tilde{\boldsymbol{p}}_i(0)\right) = 0$. Thus,

$$\begin{aligned}V(0) =& \frac{1}{2}\sum_{i=1}^{N}\sum_{j=1}^{N} a_{ij}\Psi\left(\left\|\hat{\boldsymbol{p}}_{ij}\right\|\right) < M\Psi(\bar{\Delta})\\ \le& \Psi(\hat{\Delta}) = PQ = \lambda^{\min}.\end{aligned} \tag{22}$$

According to Eq. (16) and $V(t) \le V(0)$, one can obtain

$$V_2(t) \le V(t) \le V(0) < \Psi(\hat{\Delta}) = PQ = \lambda^{\min}. \tag{23}$$

Assuming that the maximum initial distance $\|\hat{\boldsymbol{p}}_{lm}(t)\| =$ is less than $\hat{\Delta}$. This results in $V_2(t) \ge \Psi(\|\hat{\boldsymbol{p}}_{lm}(t)\|) = PQ$, which contradicts with Eq. (23). Therefore, for any $(i,j) \in \mathcal{E}$, $\|\hat{\boldsymbol{p}}_{ij}(t)\| < \hat{\Delta}$. Since $\Psi(\|\hat{\boldsymbol{p}}_{ij}\|) \ge 0$, Eqs. (18) and (23) imply $\lambda_i\left(\tilde{\boldsymbol{p}}_i\right) \le \lambda^{\min}$. Lemma 3 guarantees $\left\|\tilde{\boldsymbol{p}}_i(t)\right\| \le (\epsilon/2)$. Overall, one has

$$\left\|\boldsymbol{p}_{ij}\right\| \le \left\|\hat{\boldsymbol{p}}_{ij}\right\| + \left\|\tilde{\boldsymbol{p}}_i\right\| + \left\|\tilde{\boldsymbol{p}}_j\right\| \le \hat{\Delta} + 2\cdot(\epsilon/2) \le \Delta. \tag{24}$$

Thus, objectives (1) and (2) in Problem 1 are fulfilled, ensuring the preservation of all communication links between adjacent UAVs. ■

Remark 10. To satisfy the inequality $M\Psi(\bar{\Delta}) \le Q$ as stated in Eq. (14), or equivalently $M\Psi(\bar{\Delta}) \le \Psi(\hat{\Delta})$, we must consider the monotonicity of the potential function. This implies that if $\bar{\Delta} = \hat{\Delta}$, there is no solution to the inequality. Consequently, we select $\hat{\Delta}$ as the upper limit of the potential function, ensuring that $\bar{\Delta} < \hat{\Delta} < \Delta$.

Remark 11. The connectivity preservation controller can be designed as follows:

(1) determine the number of edges M based on the structure of graph;
(2) select Q to meet the inequality (14);
(3) set P by the equality in Eq. (15).

3.2. Attitude controller design

The distributed position controller with connectivity preservation is developed in the previous subsection. This subsection proposed a finite-time attitude controller. Considering that the connectivity preservation control requires the realization of communication distance constraints, rapid attitude control becomes essential [34,38]. Notably, finite-time control offers a distinct advantage due to its swift convergence properties. A finite-time attitude-tracking controller is proposed in this subsection. By solving Eq. (3), the desired attitude and the virtual lift of the UAVs can be articulated as follows

$$\begin{aligned} T_i^d &= m_i\sqrt{u_{i,x}^2 + u_{i,y}^2 + u_{i,z}^2}, \\ \phi_i^d &= \arcsin\left(\frac{m_i\left(u_{i,x}\sin\psi_i^d - u_{i,y}\cos\psi_i^d\right)}{T_i^d}\right), \\ \theta_i^d &= \arctan\left(\frac{u_{i,x}\cos\psi_i^d + u_{i,y}\sin\psi_i^d}{u_{i,z}+g}\right). \end{aligned} \tag{25}$$

Given that ψ_d is a free variable, we can simplify the analysis by setting the desired yaw angle, ψ_d, to zero.

The attitude controller is outlined below:

$$\begin{aligned} \tau_{i,\phi} &= -k_1\frac{J_{i,\phi}}{l_i}(\phi_i - \phi_i^d + \mathrm{sig}^{\gamma_1}(\dot{\phi}_i - \dot{\phi}_i^d)) - k_2\frac{J_{i,\phi}}{l_i}\mathrm{sig}^{\gamma_2}\left(\dot{\phi}_i - \dot{\phi}_i^d\right) \\ &\quad + \frac{J_{i,\phi}}{l_i}\ddot{\phi}_i^d + K_{i,\phi}\dot{\phi}_i^d, \\ \tau_{i,\theta} &= -k_1\frac{J_{i,\theta}}{l_i}(\theta_i - \theta_i^d + \mathrm{sig}^{\gamma_1}(\dot{\theta}_i - \dot{\theta}_i^d)) - k_2\frac{J_{i,\theta}}{l_i}\mathrm{sig}^{\gamma_2}\left(\dot{\theta}_i - \dot{\theta}_i^d\right) \\ &\quad + \frac{J_{i,\theta}}{l_i}\ddot{\theta}_i^d + K_{i,\theta}\dot{\theta}_i^d, \\ \tau_{i,\psi} &= -k_1 J_{i,\psi}c_i(\psi_i - \psi_i^d + \mathrm{sig}^{\gamma_1}(\dot{\psi}_i - \dot{\psi}_i^d)) - k_2\frac{J_{i,\psi}}{c_i}\mathrm{sig}^{\gamma_2}\left(\dot{\psi}_i - \dot{\psi}_i^d\right) \\ &\quad + \frac{J_{i,\psi}}{c_i}\ddot{\psi}_i^d + \frac{K_{i,\psi}}{c_i}\dot{\psi}_i^d, \end{aligned} \tag{26}$$

where $\mathrm{sig}^{\alpha}(x) = \mathrm{sign}(x)|x|^{\alpha}$ and $\alpha > 0$.

Now, we have the following result.

Theorem 2. *For the attitude dynamic model as described in Eq. (5), if we apply the controller defined in Eq. (26) and guarantee the parameters satisfy theconditions* $0 < \gamma_1 < 1, \gamma_2 = 2\gamma_1/(1+\gamma_1), k_1 > 0, k_2 > 0$, *then we can achieve desired attitude tracking within a finite time, that is,* $(\phi_i, \theta_i, \psi_i)^T \to (\phi_i^d, \theta_i^d, \psi_i^d)^T$ *as* $t \to \infty$.

Proof. Due to the similarity in control methods for roll, pitch, and yaw angles, we will focus on demonstrating the convergence proof exclusively for the roll angle. The tracking error is expressed as follows:

$$e_{i,\phi} = \phi_i - \phi_i^d, \quad i = 1, 2.....N. \tag{27}$$

By differentiating Eq. (27), one can obtain

$$\begin{aligned} \dot{e}_{i,\phi} &= \dot{\phi}_i - \dot{\phi}_i^d, \\ \ddot{e}_{i,\phi} &= \ddot{\phi}_i - \ddot{\phi}_i^d. \end{aligned} \tag{28}$$

By using controller (26), the dynamics (5) can be deduced as

$$\begin{aligned} \ddot{\phi}_i &= \frac{l_i}{J_{i,\phi}}(-k_1\frac{J_{i,\phi}}{l_i}(e_{i,\phi} + \mathrm{sig}^{\gamma_1}(\dot{e}_{i,\phi})) - k_2\frac{J_{i,\phi}}{l_i}\mathrm{sig}^{\gamma_2}\left(\dot{\phi}_i - \dot{\phi}_i^d\right) \\ &\quad + \frac{J_{i,\phi}}{l_i}\ddot{\phi}_i^d + K_{i,\phi}\dot{\phi}_i^d) - \frac{K_{i,\phi}l_i}{J_{i,\phi}}\dot{\phi}_i \end{aligned} \tag{29}$$

Substituting (29) into (28) yields

$$\begin{aligned} \ddot{e}_{i,\phi} &= \frac{l_i}{J_{i,\phi}}(-k_1\frac{J_{i,\phi}}{l_i}(e_{i,\phi} + \mathrm{sig}^{\gamma_1}(\dot{e}_{i,\phi})) - k_2\frac{J_{i,\phi}}{l_i}\mathrm{sig}^{\gamma_2}\left(\dot{\phi}_i - \dot{\phi}_i^d\right) \\ &\quad + \frac{J_{i,\phi}}{l_i}\ddot{\phi}_i^d + K_{i,\phi}\dot{\phi}_i^d) - \frac{K_{i,\phi}l_i}{J_{i,\phi}}\dot{\phi}_i - \ddot{\phi}_i^d \\ &= -k_1(e_{i,\phi} + \mathrm{sig}^{\gamma_1}(\dot{e}_{i,\phi})) - k_2\mathrm{sig}^{\gamma_2}\left(\dot{e}_{i,\phi}\right) - \frac{l_i K_{i,\phi}}{J_{i,\phi}}\dot{e}_{i,\phi} \end{aligned} \tag{30}$$

The Lyapunov function is designed as

$$W = \frac{1}{2}\dot{e}_{i,\phi}^2 + \frac{1}{2}k_1 {e_{i,\phi}}^2 \tag{31}$$

where $k_1 > 0$.

The derivative of (31) is

$$\dot{W} = \dot{e}_{i,\phi}\ddot{e}_{i,\phi} + k_1\dot{e}_{i,\phi}e_{i,\phi} \tag{32}$$

Proving the stability of a finite-time controller involves two steps: (1) Demonstrating that system (28) exhibits global asymptotic stability; (2) Establishing the finite-time stability of the attitude system described in Eq. (28).

Step 1: Global asymptotic stability analysis.

Substituting (30) into (32) leads to

$$\begin{aligned} \dot{W} &= \dot{e}_{i,\phi}\ddot{e}_{i,\phi} + k_1\dot{e}_{i,\phi}e_{i,\phi} \\ &= \dot{e}_{i,\phi}(-k_1(e_{i,\phi} + \mathrm{sig}^{\gamma_1}(\dot{e}_{i,\phi})) - k_2\mathrm{sig}^{\gamma_2}\left(\dot{e}_{i,\phi}\right) - \frac{l_i K_{i,\phi}}{J_{i,1}}\dot{e}_{i,\phi}) + k_1\dot{e}_{i,\phi}e_{i,\phi} \\ &= -\dot{e}_{i,\phi}(k_1\,\mathrm{sig}^{\gamma_1}(\dot{e}_{i,\phi}) + k_2\mathrm{sig}^{\gamma_2}\left(\dot{e}_{i,\phi}\right) + \frac{l_i K_{i,\phi}}{J_{i,1}}\dot{e}_{i,\phi}) \\ &= -k_1\left|\dot{e}_{i,\phi}\right|^{\gamma_1+1} - k_2\left|\dot{e}_{i,\phi}\right|^{\gamma_2+1} - \frac{l_i K_{i,\phi}}{J_{i,\phi}}\dot{e}_{i,\phi}^2 \end{aligned} \tag{33}$$

In order to analyze the stability of attitude subsystem, two cases $\dot{e}_{i,\phi} \neq 0$ and $\dot{e}_{i,\phi} = 0$, will be considered.

(1) If $\dot{e}_{i,\phi} \neq 0$, system (33) clearly satisfies $\dot{W} < 0$, so system (28) is stable.

(2) If $\dot{e}_{i,\phi} = 0$, we can define the invariant set as $\Psi = \{(e_{i,\phi}, \dot{e}_{i,\phi}) | W_g \equiv 0\}$. Clearly, if and only if $\dot{e}_{i,\phi} \equiv 0, e_{i,\phi} \equiv 0$, $\dot{W} \equiv 0$. By applying LaSalle's invariance principle, we have $(e_{i,\phi}, \dot{e}_{i,\phi}) \to 0$ as $t \to 0$. Consequently, it is affirmed that system (28) exhibits global asymptotic stability.

Step 2: The finite-time stability analysis.

Reformulating the system (28) as follows:

$$\begin{aligned} \dot{e}_{i,\phi} &= \dot{\phi}_i - \dot{\phi}_i^d \\ \ddot{e}_{i,\phi} &= -k_1\left|\dot{e}_{i,\phi}\right|^{\gamma_1+1} - k_2\left|\dot{e}_{i,\phi}\right|^{\gamma_2+1} + \hat{f}(\dot{e}_{i,\phi}) \end{aligned} \tag{34}$$

where $\hat{f}(\dot{e}_{i,\phi}) = -\frac{K_{i,\phi}l_i}{J_{i,\phi}}\dot{e}_{i,\phi}$.

Substituting the linear part of system (34) into (32), we have

$$\begin{aligned} \dot{W} &= \dot{e}_{i,\phi}\ddot{e}_{i,\phi} + k_1\dot{e}_{i,\phi}e_{i,\phi} \\ &= -\dot{e}_{i,\phi}(k_1\,\mathrm{sig}^{\gamma_1}(\dot{e}_{i,\phi}) + k_2\mathrm{sig}^{\gamma_2}\left(\dot{e}_{i,\phi}\right)) \\ &= -k_1\left|\dot{e}_{i,\phi}\right|^{\gamma_1+1} - k_2\left|\dot{e}_{i,\phi}\right|^{\gamma_2+1} \end{aligned} \tag{35}$$

Similar to the first step, the linear part of system (35) is asymptotically stable. Because $0 < \gamma_1 < 1, \gamma_2 = 2\gamma_1/(1+\gamma_1)$, the linear part

of system (35) is homogeneous of degree $h = \frac{(\gamma_1-1)}{2} < 0$ concerning dilation $s_1 = 1, s_2 = \frac{(\gamma_1+1)}{2}$.

For the nonlinear part of the system (35), it satisfies Lemma 2. For any $\dot{e}_{i,\phi} \neq 0$, it has

$$\begin{aligned}\lim_{\varepsilon\to 0}\frac{\hat{f}\left(\varepsilon^{s_2}\dot{e}_{i,\phi}\right)}{\varepsilon^{s_2+h}} &= \lim_{\varepsilon\to 0}\frac{-\frac{K_{i,\phi}l_i}{J_{i,\phi}}\varepsilon^{s_2}\dot{e}_{i,\phi}}{\varepsilon^{s_2+h}} \\ &= \lim_{\varepsilon\to 0}\left(-\frac{K_{i,\phi}l_i}{J_{i,\phi}}\varepsilon^{-h}\dot{e}_{i,\phi}\right) \\ &= 0.\end{aligned} \tag{36}$$

By Lemma 2, the system (34) exhibits local finite-time stability. Overall, the characteristics of the system (28) include both global asymptotic stability and local finite-time stability. These features together contribute to the global finite-time stability of the attitude controller. ■

Remark 12. Since explicit expressions for the desired attitude angular velocity and angular acceleration are not provided, they are determined within the application using a differentiator.

Remark 13. The attitude controller presented in this paper operates within a finite time frame but may face challenges due to frictional oscillations. The control of fractional-order systems characterized by input saturation and unknown nonlinear time delays was studied in [39,40]. This approach successfully alleviates issues related to both frictional oscillations and unknown disturbances.

Remark 14. The stability of the position controller was established in the previous subsection, and the attitude controller was stabilized in this subsection. In conclusion, the connectivity preserving control law for multiple UAVs introduced in this paper effectively preserves the graph's connectivity.

4. Simulations

In this section, we assess the effectiveness of the proposed connectivity preservation control method through numerical simulations. This section contains two primary subsections: the first involves simulation experiments conducted with a group of five UAVs, and the second entails a comparative simulation between the proposed method and another previously proposed method [22].

4.1. Simulation of five UAVs

Consider a simulation with five UAVs, where $m_i = 0.5$ kg, $L_i = [l_i,\ l_i]^\top = [0.3,\ 0.3]^\top$, $J_i = [J_{i,\phi},\ J_{i,\theta}, J_{i,\psi}]^\top = [0.0025, 0.0027, 0.0028]^\top$, $K_i = [K_{i,\phi},\ K_{i,\theta},\ K_{i,\psi}]^\top = [0.01, 0.01, 0.01]^\top$, $c_i = 0.3,\ i = 1,2,3,4,5$. Five UAVs' initial positions are $\boldsymbol{p}_1(0) = [10,0,2]^\top$ m, $\boldsymbol{p}_2(0) = [-2,5,1]^\top$m, $\boldsymbol{p}_3(0) = [-1,-2,1]^\top$ m, $\boldsymbol{p}_4(0) = [-9,2,1]^\top$ m, $\boldsymbol{p}_5(0) = [-10,-7,1]^\top$ m. The initial velocities are $\boldsymbol{v}_i(0) = [0,0,0]^\top$ (m/s), $i = 1,2,3,4,5$. The desired relative positions are $\boldsymbol{p}_1^d = [0,0,0]$, $\boldsymbol{p}_2^d = [-10,10,0]$, $\boldsymbol{p}_3^d = [-10,-10,0]$, $\boldsymbol{p}_4^d = [-20,10,0]$, $\boldsymbol{p}_5^d = [-20,-10,0]$, and the desired distances are given as $\boldsymbol{d} = [d_{12}, d_{13}, d_{14}, d_{15}] = [10\sqrt{2}, 10\sqrt{2}, 10\sqrt{5}, 10\sqrt{5}]$ m. The communication radius of each UAV is $\Delta = 35$ m. The initial attitudes are $\boldsymbol{\Phi}_i(0) = [0,0,0]^\top$, $i = 1,2,3,4,5$, the attitude angular velocities are $\boldsymbol{\omega}_i(0) = [0,0,0]^\top$, $i = 1,2,3,4,5$. The input saturation constraint in each direction is $\bar{\boldsymbol{u}}_i = [0.5,0.5,0.5]^T$ N. The radius for connectivity preserving is $\Delta = 35$. It is clear that the above conditions can fully satisfy Assumptions 1–4. Select $Q = 125000$, $P = 0.000001$, $\alpha = 0.2$, $\beta = 0.1$ as the control gain of the formation controller (9), (11), and (13). The control parameters (26) are set as follows: $k_1 = 5$, $k_2 = 5.5$, $\gamma_1 = 0.6$, $\gamma_2 = 0.75$. Fig. 3 illustrates the graph of the five UAVs.

Fig. 4 presents the distances between UAV 1 and other UAVs, where the red line marks the maximum communication range, and the black line indicates the minimum collision avoidance distance for the UAVs. The figure shows that the distances $\|\boldsymbol{p}_{12}\|$, $\|\boldsymbol{p}_{13}\|$, $\|\boldsymbol{p}_{14}\|$, $\|\boldsymbol{p}_{15}\|$ remain below the UAVs' maximum communication range, thereby preserving graph connectivity. Fig. 5 reveals that the UAV–proxy distance errors do not exceed 6 m and eventually reduce to zero. Fig. 6 signifies that the UAVs' velocities ultimately reduce to zero. Furthermore, Fig. 7 confirms that the UAV–proxy velocity errors also eventually diminish to zero, affirming that the UAV's velocities successfully track those of their virtual proxies. Fig. 8 displays the virtual control inputs exerted on each UAV, highlighting that the maximum amplitude of these control inputs stays below 0.5 N, thus adhering to the specified saturation constraints.

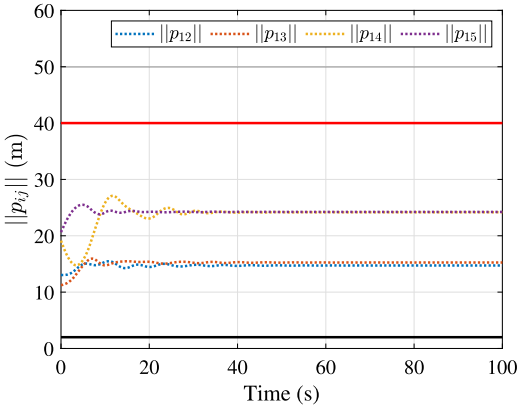

Fig. 4. The distances between UAVs.

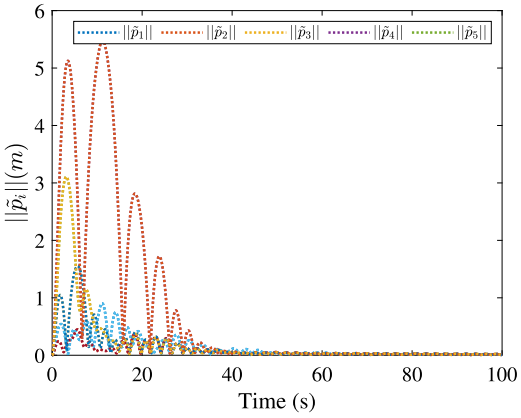

Fig. 5. The distances between UAVs and proxies.

Fig. 9 shows that attitude angles converge to zero. Since the control force applied is maintained under 0.5 N, suggesting that the required lifts and attitudes adjustments are minimal, thereby leading to modest alterations in the angles. Fig. 10 reveals a trend where the attitude angular error progressively diminishes to zero, confirming that the attitude angles align effectively with the desired values. This reinforces the observation that the attitude angles stabilize to their desired attitude.

4.2. Comparison with related literature

In this subsection, we use the same initial conditions to compare the connectivity preservation control algorithm, based on indirect coupling proposed in this paper, with the method outlined in [22]. We will choose three UAVs for numerical simulation, and the initial conditions are set as follows: $\boldsymbol{p}_1(0) = [10,0,2]^\top$ m, $\boldsymbol{p}_2(0) = [-2,5,1]^\top$m, $\boldsymbol{p}_3(0) = [-1,-2,1]^\top$ m, $\boldsymbol{v}_1(0) = [-2,0.1,0]^\top$ (m/s), $\boldsymbol{v}_2(0) = [3,0.4,0]^\top$ (m/s),

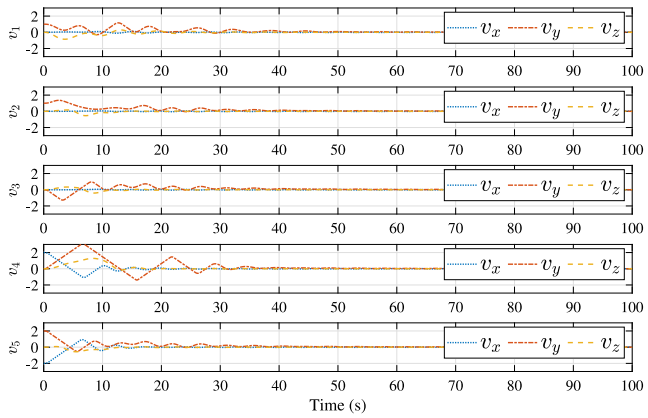

Fig. 6. The velocities of UAVs.

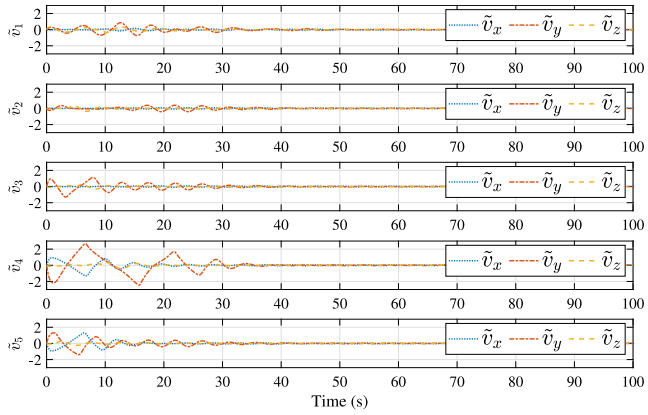

Fig. 7. The velocity errors between UAVs and proxies.

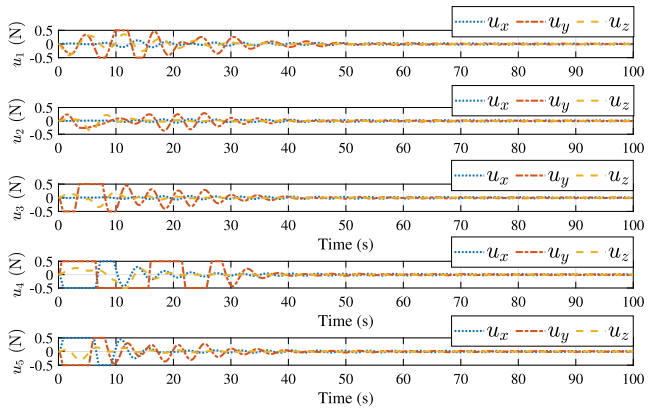

Fig. 8. The virtual control inputs.

$\boldsymbol{v}_3(0) = [7, 0.1, 0]^{\top}$ (m/s). The radius for connectivity preserving is $\Delta = 35$. Fig. 11 illustrates the graph of the three UAVs.

The desired formation is given as follows:

$$\begin{aligned}
\boldsymbol{p}_{12}^{d} &= [-10\cos\left(\frac{5\pi}{6}\right), 0, 10 - 10\sin\left(\frac{-\pi}{6}\right)]^{T}, \\
\boldsymbol{p}_{13}^{d} &= [-10\cos\left(\frac{-\pi}{6}\right), 0, 10 - 10\sin\left(\frac{-\pi}{6}\right)]^{T}, \\
\boldsymbol{p}_{23}^{d} &= \left[10\cos\left(\frac{5\pi}{6}\right) - 10\cos\left(\frac{-\pi}{6}\right), 0, 10\sin\left(\frac{-\pi}{6}\right) - 10\sin\left(\frac{-\pi}{6}\right)\right]^{T}.
\end{aligned} \tag{37}$$

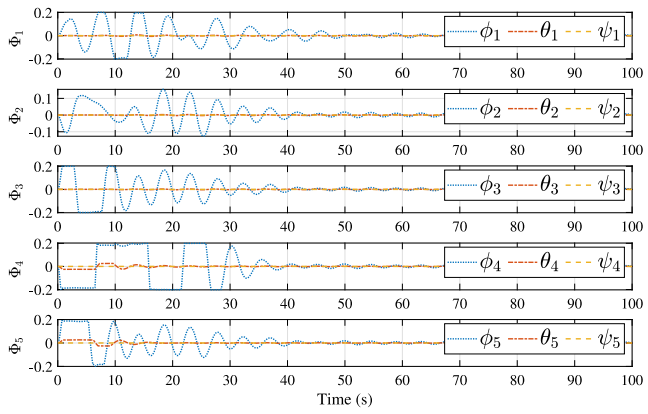

Fig. 9. The attitude of five UAV.

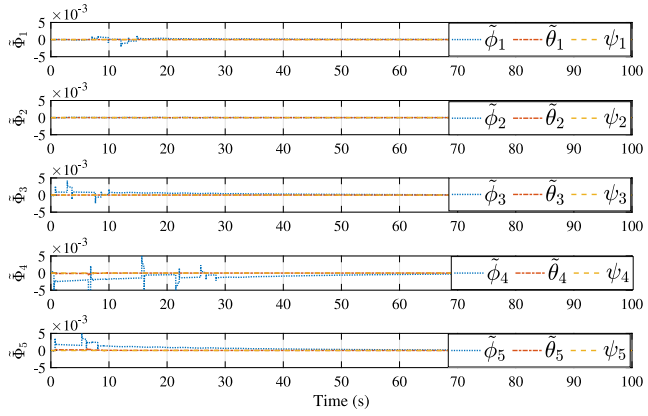

Fig. 10. The attitude tracking errors.

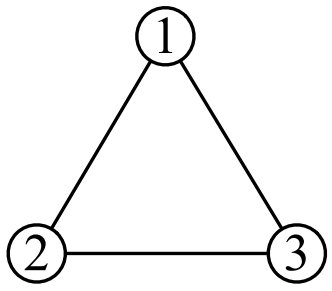

Fig. 11. The graph $\mathcal{G}$ of the three UAVs.

From this one can obtain that the desired formation distances are $\boldsymbol{d}_{ij} = [d_{12}, d_{13}, d_{23}] = [10\sqrt{3}, 10\sqrt{3}, 10\sqrt{3}]$.

The control method in [22] is :

$$\begin{aligned}
u_{i,x} &= -\sum_{j\in N_i} a_{ij}\left[k_1\chi\left(\left\|x_i - x_j - p_{ij}^{d}\right\|\right)\left(x_i - x_j - p_{ij,x}^{d}\right) + k_2\left(\dot{x}_i - \dot{x}_j\right)\right], \\
u_{i,y} &= -\sum_{j\in N_i} a_{ij}\left[k_1\chi\left(\left\|x_i - y_j - p_{ij}^{d}\right\|\right)\left(x_i - y_j - p_{ij,y}^{d}\right) + k_2\left(\dot{y}_i - \dot{y}_j\right)\right], \\
u_{i,z} &= -\sum_{j\in N_i} a_{ij}\left[k_1\chi\left(\left\|z_i - z_j - p_{ij}^{d}\right\|\right)\left(z_i - z_j - p_{ij,z}^{d}\right) + k_2\left(\dot{z}_i - \dot{z}_j\right)\right].
\end{aligned} \tag{38}$$

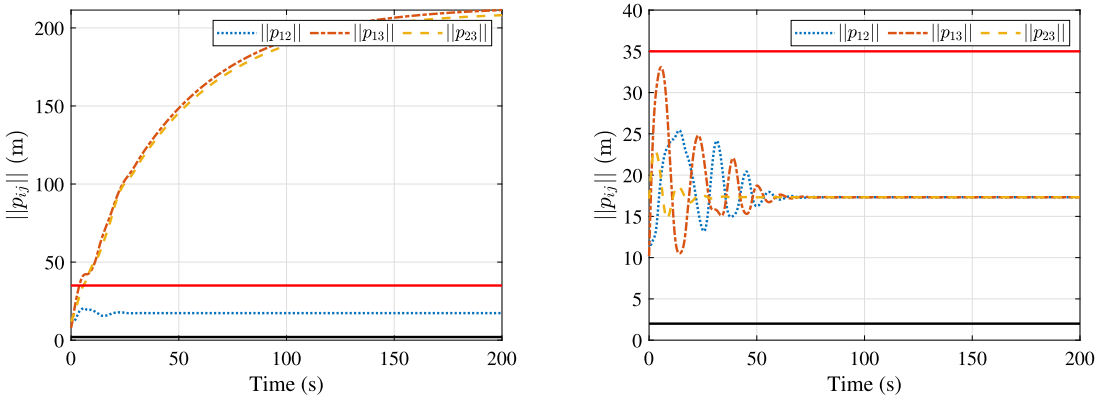

(a) The controller without input saturation [22]

(b) The proposed controller with input saturation

Fig. 12. The distance between UAVs.

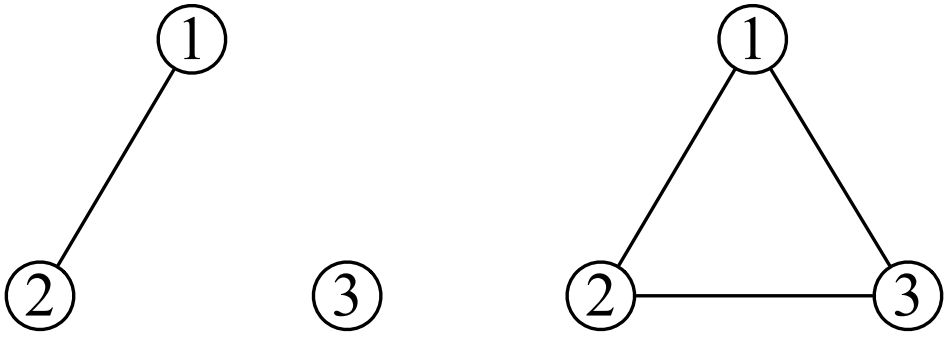

(a) The final communication graph of [22]

(b) The final communication graph of proposed controller with input saturation

Fig. 13. The final communication topology.

where $\chi(\left\|\boldsymbol{p}_i-\boldsymbol{p}_j-\boldsymbol{p}_{ij}^d\right\|)=\varphi(\left\|\boldsymbol{p}_i-\boldsymbol{p}_j-\boldsymbol{p}_{ij}^d\right\|, \Delta-\left\|\boldsymbol{p}_{ij}^d\right\|)$. The potential function $\varphi(x, R)$ in is designed as follows [22]:

$$\varphi(x,R)=\begin{cases}\dfrac{6}{R}, x\in[0,\dfrac{R}{2}),\\ \dfrac{2R-x}{(R-x)^2}, x\in[\dfrac{R}{2},R).\end{cases}$$

The control gains of formation controllers (38) is chosen as follows: $k_1=2.2, k_2=1.5$.

Fig. 12(a) how the distances between the UAVs evolve when saturation actuation is integrated into the controller described in [22]. Notably, the distances $\|\boldsymbol{p}_{13}\|$ and $\|\boldsymbol{p}_{23}\|$ exceed the maximum communication distance Δ during the formation process, leading to UAV 3 losing its links with both UAV 1 and UAV2. As depicted in Fig. 13(a), given the initial communication topology of the experiment, UAV 3 becomes an isolated point in the communication topology when it disconnects from UAV 1 and UAV 2, thereby disrupting the communication topology connectivity. Conversely, under identical initial conditions, the controller developed in this study ensures that the distances between the UAVs, as shown in Fig. 12(b), consistently remain within the designated maximum communication range, preserving network connectivity. The communication graph in Fig. 13(b) further verifies that the entire communication network remains connected. Therefore, the controller developed in this paper is proven to be more effective in preserving network connectivity compared to the strategy used in [22].

5. Conclusions

The paper presents an innovative distributed controller with connectivity preservation for multiple UAVs under input saturation. By contrast with the existing literature, our controller can preserve the UAV network connectivity even though the graph is initially assumed to be connected. The controller achieves this by applying an indirect coupling framework, ensuring that actuator saturation constraints are consistently met. A significant strength of this study is the creation of a multi-UAV formation control algorithm that simultaneously addresses input saturation and connectivity preservation. This allows the method to ensure the connectivity of the topological network even under scenarios of limited actuator capacity, proving especially beneficial for the cooperative control of small UAVs in formation. One limitation of the current study is its focus on undirected communication networks. Future research is planned to explore the challenges and solutions for preserving connectivity in directed graph networks, particularly under conditions of actuator saturation. This development could enhance the applicability and robustness of UAV cooperative control systems.

CRediT authorship contribution statement

Xianghong Xue: Writing – original draft, Project administration, Methodology, Formal analysis. **Bin Yuan:** Validation. **Yingmin Yi:** Formal analysis. **Youmin Zhang:** Writing – review & editing. **Xiaokui Yue:** Writing – review & editing. **Lingxia Mu:** Resources.

Declaration of competing interest

The authors declare that they have no known competing financial interests or personal relationships that could have appeared to influence the work reported in this paper.

Acknowledgments

This work was financed by the National Natural Science Foundation of China (Nos. 62103326, 61833013, U2013206 and 62373299), the Young Talent Fund of Xi'an Association for Science and Technology (No. 959202313034), the China Postdoctoral Science Foundation (No. 2021MD703880), the Key Research and Development Program of Shaanxi (No. 2023-YBGY-380), the Innovation Capability Support Program of Shaanxi (No. 2023-CX–01), the Scientific Research Program Funded by Shaanxi Provincial Education Department (Nos. 21JK0800 and 21JY033), the Science and Technology Foundation of the National Key Laboratory of Aerospace Flight Dynamics (No. 6142210200310) and the Natural Sciences and Engineering Research Council of Canada.

References

[1] Dorigo M, Theraulaz G, Trianni V. Swarm robotics: Past, present, and future. Proc IEEE 2021;109(7):1152–65.
[2] Meng K, Wu Q, Xu J, Chen W, Feng Z, Schober R, Swindlehurst AL. UAV-enabled integrated sensing and communication: Opportunities and challenges. IEEE Wirel Commun 2023.
[3] Huang J, Luo Y, Quan Q, Wang B, Xue X, Zhang Y. An autonomous task assignment and decision-making method for coverage path planning of multiple pesticide spraying UAVs. Comput Electron Agric 2023;212:108128.
[4] Skorobogatov G, Barrado C, Salamí E. Multiple UAV systems: a survey. Unmanned Syst 2020;8(02):149–69.
[5] Doostmohammadian M, Taghieh A, Zarrabi H. Distributed estimation approach for tracking a mobile target via formation of UAVs. IEEE Trans Autom Sci Eng 2021;19(4):3765–76.
[6] Biswas S, Behera S, Choudhury NBD. A brief review on the barriers of electric vehicle adoption and present scenario in India. In: International conference on flexible electronics for electric vehicles. Springer; 2022, p. 539–50.
[7] Doostmohammadian M. Single-bit consensus with finite-time convergence: Theory and applications. IEEE Trans Aerosp Electron Syst 2020;56(4):3332–8.
[8] Chung S-J, Paranjape AA, Dames P, Shen S, Kumar V. A survey on aerial swarm robotics. IEEE Trans Robot 2018;34(4):837–55.
[9] Liu Y, Bucknall R. A survey of formation control and motion planning of multiple unmanned vehicles. Robotica 2018;36(7):1019–47.
[10] Zavlanos MM, Pappas GJ. Potential fields for maintaining connectivity of mobile networks. IEEE Trans Robot 2007;23(4):812–6.
[11] Stephan J, Fink J, Kumar V, Ribeiro A. Concurrent control of mobility and communication in multirobot systems. IEEE Trans Robot 2017;33(5):1248–54.
[12] Wei C, Wu X, Xiao B, Wu J, Zhang C. Adaptive leader-following performance guaranteed formation control for multiple spacecraft with collision avoidance and connectivity assurance. Aerosp Sci Technol 2022;120:107266.
[13] Qiao Y, Huang X, Yang B, Geng F, Wang B, Hao M, Li S. Formation tracking control for multi-agent systems with collision avoidance and connectivity maintenance. Drones 2022;6(12):419.
[14] Khateri K, Pourgholi M, Montazeri M, Sabattini L. A comparison between decentralized local and global methods for connectivity maintenance of multi-robot networks. IEEE Robot Autom Lett 2019;4(2):633–40.
[15] Kim Y, Mesbahi M. On maximizing the second smallest eigenvalue of a state-dependent graph Laplacian. IEEE Trans Autom Control 2006;51(1):116–20.
[16] Qu Z, Li C, Lewis F. Cooperative control with distributed gain adaptation and connectivity estimation for directed networks. Internat J Robust Nonlinear Control 2014;24(3):450–76.
[17] Fang H, Wei Y, Chen J, Xin B. Flocking of second-order multiagent systems with connectivity preservation based on algebraic connectivity estimation. IEEE Trans Cybern 2016;47(4):1067–77.
[18] Ji M, Egerstedt M. Distributed coordination control of multiagent systems while preserving connectedness. IEEE Trans Robot 2007;23(4):693–703.
[19] Xue X, Yue X, Yuan J. Distributed connectivity maintenance and collision avoidance control of spacecraft formation flying. In: 2019 Chinese control conference. CCC, IEEE; 2019, p. 8265–70.
[20] Xue X, Yue X, Yuan J. Connectivity preservation and collision avoidance control for spacecraft formation flying in the presence of multiple obstacles. Adv Space Res 2021;67(11):3504–14.
[21] Yi J, Li J, Zhang Z. Fixed-time connectivity-preserving consensus of periodically disturbed nonlinear multi-agent systems with limited communication ranges. ISA Trans 2023;138:291–300.
[22] Cong Y, Du H, Jin Q, Zhu W, Lin X. Formation control for multiquadrotor aircraft: Connectivity preserving and collision avoidance. Internat J Robust Nonlinear Control 2020;30(6):2352–66.
[23] Fu M, Xu Y, Yu Z, Zhang Y, et al. Decentralized adaptive fault-tolerant cooperative control for multiple UAVs with input saturation and state constraints. Int J Aerosp Eng 2022;2022.
[24] Jiang T, Lin D, Song T. Finite-time backstepping control for quadrotors with disturbances and input constraints. IEEE Access 2018;6:62037–49.
[25] Li Z, Chen X, Xie M, Zhao Z. Adaptive fault-tolerant tracking control of flying-wing unmanned aerial vehicle with system input saturation and state constraints. Trans Inst Meas Control 2022;44(4):880–91.
[26] Li J, Wan L, Li J, Hou K. Adaptive backstepping control of quadrotor UAVs with output constraints and input saturation. Appl Sci 2023;13(15):8710.
[27] Eliker K, Grouni S, Tadjine M, Zhang W. Practical finite time adaptive robust flight control system for quad-copter UAVs. Aerosp Sci Technol 2020;98:105708.
[28] Liu B, Li A, Guo Y, Wang C. Adaptive distributed finite-time formation control for multi-UAVs under input saturation without collisions. Aerosp Sci Technol 2022;120:107252.
[29] Wen G, Duan Z, Su H, Chen G, Yu W. A connectivity-preserving flocking algorithm for multi-agent dynamical systems with bounded potential function. IET Control Theory Appl 2012;6(6):813–21.
[30] Li X, Sun D, Yang J. A bounded controller for multirobot navigation while maintaining network connectivity in the presence of obstacles. Automatica 2013;49(1):285–92.
[31] Yang Y, Constantinescu D, Shi Y. Connectivity-preserving consensus of multi-agent systems with bounded actuation. 2018, arXiv preprint arXiv:1803.09309.
[32] Zou Y, Meng Z. Immersion and invariance-based adaptive controller for quadrotor systems. IEEE Trans Syst Man Cybern: Syst 2018;49(11):2288–97.
[33] Kendoul F, Yu Z, Nonami K. Guidance and nonlinear control system for autonomous flight of minirotorcraft unmanned aerial vehicles. J Field Robotics 2010;27(3):311–34.
[34] Zhao B, Xian B, Zhang Y, Zhang X. Nonlinear robust adaptive tracking control of a quadrotor UAV via immersion and invariance methodology. IEEE Trans Ind Electron 2014;62(5):2891–902.
[35] Mesbahi M, Egerstedt M. Graph theoretic methods in multiagent networks, vol. 33, Princeton University Press; 2010.
[36] Hong Y, Xu Y, Huang J. Finite-time control for robot manipulators. Systems Control Lett 2002;46(4):243–53.
[37] Yang Y, Shi Y, Constantinescu D. Connectivity-preserving synchronization of time-delay Euler-Lagrange networks with bounded actuation. IEEE Trans Cybern 2021;51(7):3469–82.
[38] Wang F, Gao H, Wang K, Zhou C, Zong Q, Hua C. Disturbance observer-based finite-time control design for a quadrotor UAV with external disturbance. IEEE Trans Aerosp Electron Syst 2020;57(2):834–47.
[39] Zouari F, Boubellouta A. Neural approximation-based adaptive control for pure-feedback fractional-order systems with output constraints and actuator nonlinearities. In: Advanced synchronization control and bifurcation of chaotic fractional-order systems. IGI Global; 2018, p. 468–95.
[40] Zouari F, Boubellouta A. Adaptive neural control for unknown nonlinear time-delay fractional-order systems with input saturation. In: Advanced synchronization control and bifurcation of chaotic fractional-order systems. IGI Global; 2018, p. 54–98.